In situ doping of catalyst-free InAs nanowires

2012 Nanotechnology 23 505708

(http://iopscience.iop.org/0957-4484/23/50/505708)

Nanotechnology **23** (2012) 505708 (6pp) doi:10.1088/0957-4484/23/50/505708

In situ doping of catalyst-free InAs nanowires

Hesham Ghoneim[1], Philipp Mensch[1], Heinz Schmid[1], Cedric D Bessire[1], Reto Rhyner[2], Andreas Schenk[2], Charles Rettner[3], Siegfried Karg[1], Kirsten E Moselund[1], Heike Riel[1] and Mikael T Björk[1,4]

[1] IBM Research—Zürich, Säumerstrasse 4, 8803 Rüschlikon, Switzerland
[2] Integrated Systems Laboratory, ETH Zürich, Gloriastr. 35, 8092 Zürich, Switzerland
[3] IBM Research—Almaden, 650 Harry Road, San Jose, CA 95120-6099, USA

E-mail: mikael.t.bjork@gmail.com

Received 24 August 2012, in final form 25 October 2012
Published 27 November 2012
Online at stacks.iop.org/Nano/23/505708

Abstract
We report on *in situ* doping of InAs nanowires grown by metal–organic vapor-phase epitaxy without any catalyst particles. The effects of various dopant precursors (Si_2H_6, H_2S, DETe, CBr_4) on the nanowire morphology and the axial and radial growth rates are investigated to select dopants that enable control of the conductivity in a broad range and that concomitantly lead to favorable nanowire growth. In addition, the resistivity of individual wires was measured for different gas-phase concentrations of the dopants selected, and the doping density and mobility were extracted. We find that by using Si_2H_6 axially and radially uniform doping densities up to 7×10^{19} cm^{-3} can be obtained without affecting the morphology or growth rates. For sulfur-doped InAs nanowires, we find that the distribution coefficient depends on the growth conditions, making S doping more difficult to control than Si doping. Moreover, above a critical sulfur gas-phase concentration, compensation takes place, limiting the maximum doping level to 2×10^{19} cm^{-3}. Finally, we extract the specific contact resistivity as a function of doping concentration for Ti and Ni contacts.

S Online supplementary data available from stacks.iop.org/Nano/23/505708/mmedia

(Some figures may appear in colour only in the online journal)

1. Introduction

One of the main benefits of semiconductor materials is the possibility to change both the charge-carrier type and the density from insulator to near metal by adding dopants in controlled amounts. This ability allows the realization of a vast range of electronic devices, and becomes even more important as semiconductor device dimensions are scaled down. In CMOS technology, for instance, improved control over source and drain doping is essential for device performance. In addition, the trend towards nonplanar devices based on fins [1] and nanowires [2] adds further challenges to doping control. *In situ* doping has been demonstrated as an effective method to achieve control over doping levels and, in particular, the junction abruptness in nanowires, which is especially important for tunnel diodes [3, 4] and tunnel FETs [5, 6]. However, the addition of doping during nanowire growth often influences the axial and radial growth rates, resulting in inhomogeneous radial and axial doping profiles [7]. Here we report on n-type *in situ* doping of InAs nanowires grown in oxide-mask openings on silicon wafers without any catalyst particles. We study the effect of various group-IV and group-VI doping species on the nanowire morphology, the axial and radial growth rates and the electrical properties.

2. Experimental details

The nanowires used here were grown by metal–organic vapor-phase epitaxy (MOVPE) using trimethyl-indium (TMIn) and tertiary-butyl-arsine (TBAs) precursors. The ⟨111⟩ Si

[4] Present address: QuNano AB, Scheelevaegen 17, 22370 Lund, Sweden.

substrates used were masked with a 65 nm-thick SiO_x layer deposited by plasma-enhanced chemical vapor deposition (PECVD). Subsequently, mask openings to the Si surface were fabricated by electron-beam lithography and oxide etching in buffered hydrofluoric acid (BHF). We used a layout consisting of hexagonally patterned and 1 μm-spaced 150 nm-diameter openings. By using very large arrays (5000 $\times$ 5000 openings) the radial growth rate could be reduced to zero so that effectively only an axial extension of the wires during the growth was possible, as already demonstrated for conditions without the addition of dopants [8]. The growth was carried out at 520 °C at a TMIn molar flow of $\Phi_{\mathrm{TMIn}} = 0.38$ μmol min^{-1} and a V/III ratio of 20 unless stated otherwise, yielding an axial growth rate of 50 nm min^{-1}. Under these growth conditions there is no catalyst present on top of the wire [8]. To investigate the n-type doping incorporation into the InAs nanowires, diethyl telluride (DETe), disilane (Si_2H_6), hydrogen sulfide (H_2S) or carbon tetrabromide (CBr_4) was injected into the chamber at $\Phi_{\mathrm{dop}}/(\Phi_{\mathrm{TMIn}} + \Phi_{\mathrm{TBAs}})$ ratios ranging from 10^{-5} to 10^{-2}.

For electrical characterization nanowires having lengths of approximately 3 μm and diameters in the range of 100–150 nm were mechanically transferred from the growth substrates to Si substrates covered with 100 nm-thick SiO_2 layers and pre-patterned Au pads. The Au pads were used to optically record the position of the nanowires so that electron-beam lithography could be used to pattern four contacts to each individual nanowire. After developing the PMMA resist in isopropanol/H_2O, a short O_2-plasma cleaning was carried out to remove any resist residues, followed by a short dip in BHF and subsequent loading into an evaporation chamber, where 70 nm Ti and 80 nm Au or 150 nm Ni were evaporated. Electrical characterization was performed by two-point transmission line measurements and four-point probe measurements with the spacing between the electrodes varying from 120 to 650 nm. Similar processing steps were used to fabricate the devices for measuring the Seebeck coefficient (see the supplemental information available at stacks.iop.org/Nano/23/505708/mmedia). After the electrical measurements, scanning electron microscope (SEM) images were recorded to obtain the nanowire diameter and the distance between the contact leads for the data analysis.

3. Results and discussion

3.1. The effect of doping on nanowire growth

The addition of dopants during growth can affect both the axial, $\langle 111 \rangle$, and radial, $\langle 1\bar{1}0 \rangle$, growth rates as well as the morphology and nucleation. We observe that when using CBr_4 the nucleation of nanowires is drastically reduced at $\Phi_{\mathrm{CBr_4}}/(\Phi_{\mathrm{TMIn}} + \Phi_{\mathrm{TBAs}})$ ratios larger than 10^{-3}. The addition of the slightest amount of DETe ($\Phi_{\mathrm{DETe}}/(\Phi_{\mathrm{TMIn}} + \Phi_{\mathrm{TBAs}}) \sim 10^{-6}$) completely inhibits $\langle 111 \rangle$ growth and only $\langle 1\bar{1}0 \rangle$ growth is possible, making DETe unsuitable for *in situ* doping of nanowires unless pure shell doping is needed. In contrast, doping of InAs nanowires with hydrogen sulfide (H_2S) shows

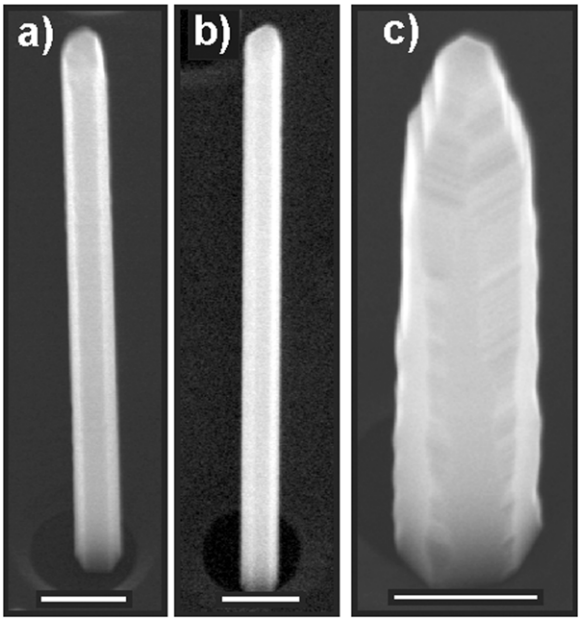

Figure 1. The effects of sulfur and silicon doping on InAs nanowire growth. (a) Sulfur-doped nanowire. For all doping concentrations used, no change in morphology is observed. (b) Si-doped InAs nanowire. For Si concentrations up to $\Phi_{\mathrm{Si_2H_6}}/(\Phi_{\mathrm{TMIn}} + \Phi_{\mathrm{TBAs}}) = 2 \times 10^{-3}$ the nanowire morphology and radial growth are unchanged with respect to the undoped case. (c) Drastic changes in the axial and radial growth as well as in the morphology are observed for Si_2H_6 molar flows above $\Phi_{\mathrm{Si_2H_6}}/(\Phi_{\mathrm{TMIn}} + \Phi_{\mathrm{TBAs}}) = 2 \times 10^{-3}$. The scale bars are 200 nm.

no change in the growth rate, morphology or nucleation as compared to undoped wires, even for $\Phi_{\mathrm{H_2S}}/(\Phi_{\mathrm{TMIn}} + \Phi_{\mathrm{TBAs}})$ ratios as large as 10^{-2}. Figure 1(a) displays a sulfur-doped wire, in which smooth $\langle 1\bar{1}0 \rangle$ side wall facets are seen. The same observations are made when using Si_2H_6 (figure 1(b)); however, at $\Phi_{\mathrm{Si_2H_6}}/(\Phi_{\mathrm{TMIn}} + \Phi_{\mathrm{TBAs}})$ ratios above 2×10^{-3} the $\langle 111 \rangle$ growth rate drops, whereas the $\langle 1\bar{1}0 \rangle$ growth rate increases to several 10 nm min^{-1}. In addition, the side walls appear to be tapered (figure 1(c)) because of the addition of a critical amount of Si atoms, which reduces the diffusion length of TMIn on the $\langle 1\bar{1}0 \rangle$ surface. These effects become more pronounced with increasing $\Phi_{\mathrm{Si_2H_6}}/(\Phi_{\mathrm{TMIn}} + \Phi_{\mathrm{TBAs}})$ ratios above 2×10^{-3}. A change in the $\langle 111 \rangle$ and $\langle 1\bar{1}0 \rangle$ growth rates upon Si doping of InAs was also observed by Wirths *et al* [9] for selective area growth performed at 650 °C in N_2.

3.2. Resistivity measurements of C-, Si- and S-doped nanowires

To study the electrical properties of the C-, Si- and S-doped InAs nanowires, two- and four-point-probe electrical measurements were performed. The resistance was observed to increase linearly with nanowire length for all doping species, indicating a uniform conductance and therefore doping incorporation along the wire. As the wires are grown in very large arrays, radial growth is absent (for the conditions and doping species identified above) and hence no radial doping profile is expected. However, to exclude a radial doping profile, the samples were thinned

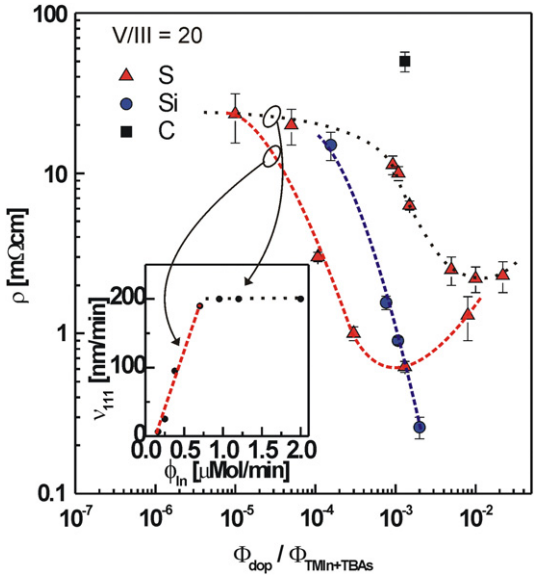

Figure 2. Doping incorporation. The measured resistivities of doped InAs nanowires versus doping concentration in the gas phase for S (red triangles), Si (blue circles) and C (black square) doping atoms. The dotted black curve shows the incorporation of S for a TMIn molar flow of $\Phi_{TMIn} = 0.95$ μmol min^{-1}, whereas the dashed red line shows the same for a TMIn molar flow of $\Phi_{TMIn} = 0.38$ μmol min^{-1}. The inset shows the axial growth rate as a function of TMIn flow, indicating two distinct regions of growth behavior corresponding to those identified in the main plot. The Si_2H_6 curve (dashed blue) exhibits no dependence on the TMIn molar flow.

down to ∼20–30 nm by wet chemical etching in a citric acid/peroxide ($C_6H_8O_7$:H_2O_2, 10:1) solution for 10–20 s, which etched the InAs wires but left the Ni contacts intact, after which the resistivity was measured once more. The samples exhibited the same resistivity as before thinning, which confirms a uniform radial dopant distribution. In figure 2, the resistivity measured for various dopants is plotted versus $\Phi_{dop}/(\Phi_{TMIn} + \Phi_{TBAs})$. The resistivity of the non-intentionally doped nanowires was measured to be 23 mΩ cm but, as will be discussed later, this value does not correspond to the bulk resistivity in the wire. Carbon doping using CBr_4 at the maximum $\Phi_{CBr_4}/(\Phi_{TMIn} + \Phi_{TBAs})$ ratio of 10^{-3} shows an increase in resistivity to 45 mΩ cm, indicating that C is incorporated as a shallow acceptor. This is consistent with both the fact that carbon is a known amphoteric dopant in III/V materials and that at our conditions ⟨111⟩ growth is V-limited [8], forcing incorporation on the As site. No further measurements using CBr_4 at reduced flows were conducted as we did not expect a significant gain over Si and S doping.

By employing Si_2H_6 doping instead, we were able to significantly reduce the nanowire resistivity. A sharp decrease in resistivity with increasing Si_2H_6 concentration was observed (circular symbols in figure 2), yielding a minimum value of 0.26 mΩ cm at $\Phi_{Si_2H_6}/(\Phi_{TMIn}+\Phi_{TBAs}) = 2 \times 10^{-3}$, which is the highest ratio possible without changing the morphology, as discussed previously. H_2S doping (lower curve with triangular symbols in figure 2) shows a similar trend but reaches a minimum resistivity value of 0.6 mΩ cm at $\Phi_{H_2S}/(\Phi_{TMIn} + \Phi_{TBAs}) = 10^{-3}$, after which an increase in resistivity is observed. The second curve for H_2S (upper curve with triangular symbols in figure 2) is measured for wires grown with an identical V/III ratio, but at a TMIn flow of 0.95 μmol min^{-1}. The resistivity measured is higher overall than for the low TMIn molar flow data for all H_2S concentrations used. We attribute the difference between these two curves to a change in the distribution coefficient of H_2S. In the inset of figure 2 the axial growth rate, ν_{111}, is displayed as a function of TMIn flow [8], showing two distinct regions corresponding to the conditions used for the two sulfur data sets in figure 2. During growth in the high TMIn flow region ($\Phi_{TMIn} = 0.95$ μmol min^{-1}), the V/III ratio is locally high, making sulfur incorporation (on the As site) less favorable because of a reduced distribution coefficient [10]. In the low TMIn flow regime ($\Phi_{TMIn} = 0.38$ μmol min^{-1}), ⟨111⟩ growth is V-limited [8], and in this case the local V/III ratio is lower than in the high TMIn flow regime. In the latter case, sulfur incorporation therefore becomes more favorable (higher distribution coefficient). Such a dependence of the doping incorporation on the V/III ratio is also known, for example, from Zn doping of GaAs [11, 12]. Interestingly, the distribution coefficient of Si_2H_6 does not exhibit this dependence. We also note that when the low TMIn flow data set for H_2S starts showing increasing resistivity values, the high TMIn flow data set also saturates. At high $\Phi_{H_2S}/(\Phi_{TMIn} + \Phi_{TBAs})$ ratios, both curves seem to reach the same resistivity values. Because the minimum resistivity values of the two curves are dissimilar, it is unlikely that the ultimate increase in resistivity is due to auto-compensation driven by a lowering of the formation energy of native defects [13, 14], as this would always happen at a specific doping density (Fermi level position). Instead, we believe that at high sulfur to TMIn ratios, the sulfur might form a complex in the host, which causes compensation and an increase in the resistivity.

3.3. Extraction of the doping concentration and carrier mobility

The doping concentrations of the nanowires were extracted from the measured resistivity values by using three experimental reference measurements that are independent of the carrier mobility. The first method consisted of measuring the Seebeck coefficient, S, of doped InAs nanowires [15]. Experimental details of the Seebeck measurements can be found in [16] and in the supplemental information (available at stacks.iop.org/Nano/23/505708/mmedia). The bulk relation between S and N_D [17] then allowed us to deduce $N_D = 4 \times 10^{18}$ and 1×10^{18} cm^{-3} for $\Phi_{H_2S}/(\Phi_{TMIn} + \Phi_{TBAs}) = 10^{-4}$ and 10^{-3} (at high TMIn flow) and $N_D = 7 \times 10^{19}$ for $\Phi_{Si_2H_6}/(\Phi_{TMIn} + \Phi_{TBAs}) = 2 \times 10^{-3}$. Using the measured resistivities of $\rho = 0.26$, 3 and 9 mΩ cm, we then extracted carrier mobilities of $\mu_e = 344$, 520 and 545 cm^2 V^{-1} s^{-1}. The second reference method consisted of analyzing an InAs homojunction tunnel diode. The diode was made from a Si-doped InAs nanowire ($\Phi_{Si_2H_6}/(\Phi_{TMIn} + \Phi_{TBAs}) = 8 \times 10^{-4}$) on a p-type doped InAs substrate ($N_A = 1 \times 10^{19}$ cm^{-3}).

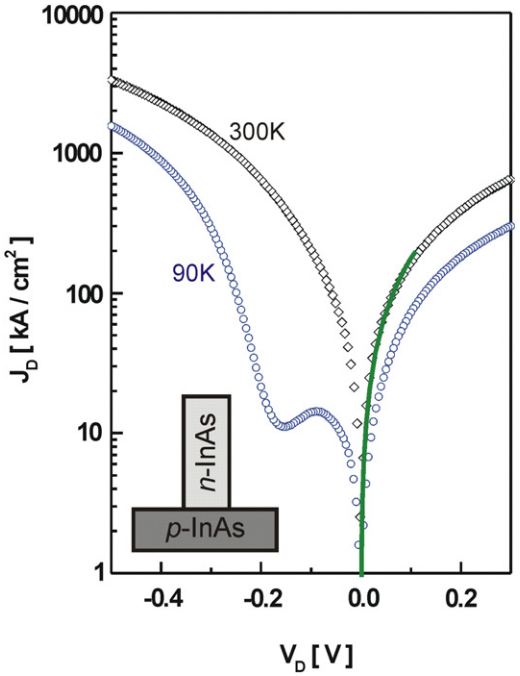

Figure 3. A vertical InAs homojunction Esaki diode. A negative differential resistance is observed at low temperature (blue circles). At room temperature (black squares) the reverse current density (positive voltage) reaches ∼300 kA cm^{-2} at 0.3 V bias. TCAD modeling of this device (solid line) was used to derive the doping density in the Si-doped InAs nanowire source region with a substrate doping of $N_A = 1 \times 10^{19}$ cm^{-3}. The green line corresponds to the best fit with $N_D = 1 \times 10^{19}$ cm^{-3}.

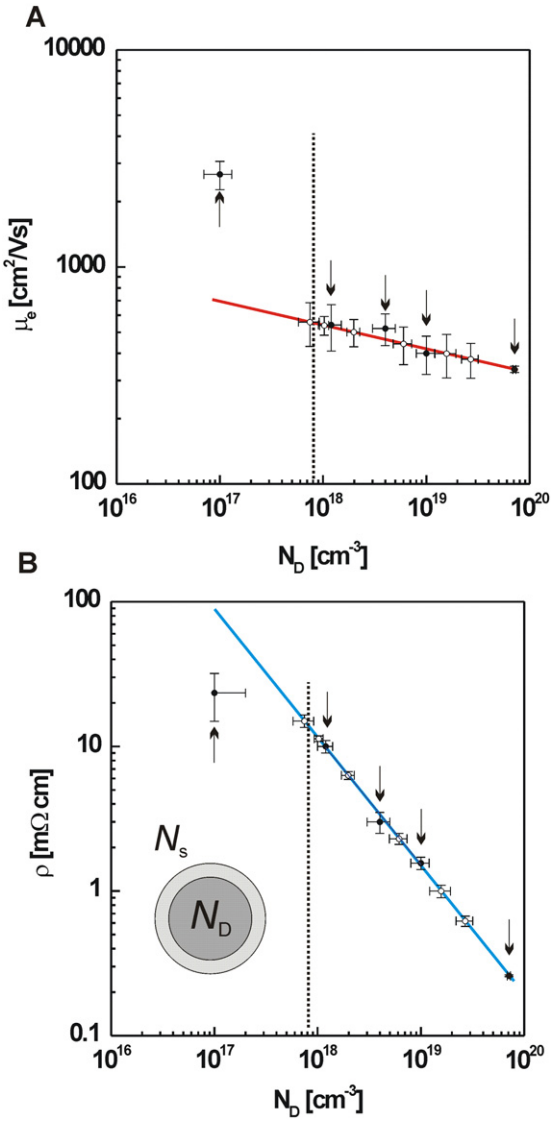

Figure 4. The doping density and mobility of InAs nanowires. (a) Electron mobility versus doping density. The mobility is calculated from the doping density and resistivity data in (b). (b) Resistivity versus doping concentration. The closed symbols are from the five reference measurements and the open symbols are from resistivity measurements. The deviation from the dashed line at lower doping concentrations is due to the inability to measure the resistivity correctly and is caused by the accumulation layer (sketched in the inset) at the nanowire surface. By extrapolation we find a value for the resistivity of undoped nanowires of 80 mΩ cm, in contrast to the measured value of 23 mΩ cm.

The electrical characteristics of such a diode are shown in figure 3 as a function of temperature.

Using TCAD simulations [18], it was possible to fit the characteristics to the experimental data for $N_D = 1 \times 10^{19}$ cm^{-3} (solid line in figure 3). Using the measured resistivity of $\rho = 1.6$ mΩ cm, we extracted a mobility of $\mu_e = 400$ cm^2 V^{-1} s^{-1}. The third reference method utilized was to fit the experimental data of an InAs/Si heterojunction tunnel diode [19] using TCAD simulations [18] with the InAs nanowire doping concentration as the only fitting parameter. From that analysis, a doping concentration of $N_D = 1 \times 10^{17}$ cm^{-3} in undoped InAs nanowires was obtained. In figure 4(a), the resulting carrier mobility versus doping density is plotted for the nanowires with the four reference values indicated by filled symbols and black arrows.

The mobility is observed to deviate from a linear trend only below $N_D = 1 \times 10^{18}$ cm^{-3}. This functional behavior is similar to the universal mobility dependence in bulk InAs [20], and is also found for the resistivity versus doping density in figure 4(b). The open symbols in figure 4(a) were obtained by calculating the mobility using the resistivity and doping density data in figure 4(b). The plot in figure 4(b) was obtained by a line fit based on three reference values (filled symbols) onto which all resistivity measurements were overlaid to obtain the corresponding doping density values. The highest doping concentration measured in the wires, 7.1×10^{19} cm^{-3}, is close to the maximum reported doping levels in bulk InAs [21]. The deviation of the resistivity for $N_D \leq 1 \times 10^{18}$ cm^{-3} from the trend at higher doping levels results from an inhomogeneous carrier profile in the wire due to an accumulation layer [22] at the surface, which prevents the correct measurement of the resistivity. The accumulation layer formed on the $\langle 1\bar{1}0 \rangle$ InAs surface typically has a sheet density of $N_S \approx 1 \times 10^{12}$ cm^{-2} [23], corresponding to a doping density of $\sim 8 \times 10^{17}$ cm^{-3} (indicated by the vertical line in figure 4) in a 10 nm-thick surface layer. Based on the results shown in figure 4(b), this doping density translates into a resistivity of 12 mΩ cm, which is lower than that of the bulk part of the

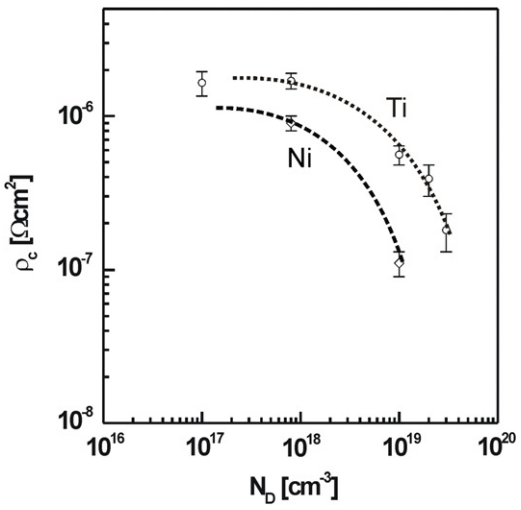

Figure 5. The specific contact resistivity. The contact resistivity versus doping density for n-doped InAs nanowires. The topmost curve is for Ti contacts and the lower one for Ni contacts.

wire. The true resistivity in the bulk of the wire is obtained by extrapolating the data in figure 4(b) to $N_D = 1 \times 10^{17}$ cm^{-3}, which yields $\rho = 60$ mΩ cm. Alternatively, we can estimate the resistivity of the low-doped sample by accounting for the area of bulk resistivity in the core (100 nm in diameter with $\rho = 60$ mΩ cm) in parallel with an accumulation layer at the surface (10 nm-thick sheet with $\rho = 12$ mΩ cm) to be $\rho = 27$ mΩ cm, which is in good agreement with the measured value of $\rho = 23$ mΩ cm. The existence of an accumulation layer at the surface is therefore the reason for the leveling off in the measured resistivity as the doping density drops below $\sim 1 \times 10^{18}$ cm^{-3}. Referring back to figure 2(a), it is therefore not until a doping density of roughly 1×10^{18} cm^{-3} has been reached in the wire that a correct measurement of the resistivity becomes possible (uniform carrier profile is reached in the wire), and a drop in resistivity versus $\Phi_{dop}/(\Phi_{TMIn} + \Phi_{TBAs})$ can be observed. The correct resistivity for undoped wires is thus $\rho = 60$ mΩ cm, which is higher than the values found for Au-catalyzed nanowires [24], but similar to values published by Wirths *et al* [9] for catalyst-free grown InAs. The extracted resistivity for undoped nanowires corresponds to a doping density of 1×10^{17} cm^{-3} and a mobility of 1000 cm^2 V^{-1} s^{-1}.

3.4. Contact resistivity

In addition to the resistivity, the specific contact resistivity was also determined from the electrical measurements. This was carried out by plotting the measured resistivity values versus the electrode spacing, and determining the intercept of the linear curves with the resistance axis. Figure 5 displays the extracted contact resistivity as a function of doping concentration for Ti- and Ni-based contacts.

It is observed that the contact resistivity decreases by an order of magnitude with increasing doping concentration, from 1.2×10^{-6} Ω cm^{-2} for undoped nanowires to 1.7×10^{-7} Ω cm^{-2} for the highest doped nanowires. In addition, Ni-based metallization schemes seem to give consistently lower contact resistivities than Ti-based schemes.

4. Conclusion

We have studied *in situ* doping of InAs nanowires grown epitaxially without any catalysts. The data show that excellent control over the n-type doping incorporation can be achieved, making it possible to obtain doping concentrations ranging from 1×10^{17} cm^{-3} (undoped) to 7×10^{19} cm^{-3}, which are comparable to the highest doping concentrations reported in bulk InAs. These doping densities are achieved without changes in the morphology or the radial growth, and are uniform, both axially and radially, in the nanowires. For very high doping flows of Si_2H_6, we observe that the radial growth and the morphology change drastically for increasing doping concentration in the gas phase. In particular, when using sulfur, compensation effects occurred at very high concentrations. We further show that the specific contact resistivity decreases by an order of magnitude with increasing doping concentration, from $\sim 1.5 \times 10^{-6}$ Ω cm^{-2} for undoped nanowires to 1.7×10^{-7} Ω cm^{-2} for the highest doped ones, and Ni-based metallization schemes give lower contact resistivities than Ti-based schemes. The results demonstrate the possibility to achieve very high doping densities in InAs nanowire structures grown with *in situ* doping, which is promising for future FET applications.

Acknowledgments

The authors gratefully acknowledge D Webb, D Caimi, N Arellano, G Zhou, E Lörtscher, A M Ionescu and M Tschudy. The research leading to these results has received funding from the European Union Seventh Framework Program (FP7/2007–2013) STEEPER under grant agreement No. [257267].

References

[1] Wu C C *et al* 2012 *IEDM Tech. Digest* **27** 1–27
[2] Bangsaruntip S *et al* 2010 *Symp. VLSI Tech.* pp 21–2
[3] Wallentin J, Persson J M, Wagner J B, Samuelson L, Deppert K and Borgström M 2010 *Nano Lett.* **10** 974
[4] Schmid H, Bessire C D, Björk M T, Schenk A and Riel H 2011 *Nano Lett.* **12** 699
[5] Schmid H, Moselund K E, Björk M T, Richter M, Ghoneim H, Bessire C D and Riel H 2011 *Proc. 69th Annual IEEE Device Research Conf.* p 181
[6] Björk M T, Knoch J, Schmid H, Riel H and Riess W 2008 *Appl. Phys. Lett.* **92** 19350
[7] Allen J E, Perea D E, Hemesath E R and Lauhon L J 2009 *Adv. Mater.* **21** 3067
[8] Björk M T, Schmid H, Breslin C, Gignac L and Riel H 2011 *J. Cryst. Growth* **344** 31
[9] Wirths S *et al* 2011 *J. Appl. Phys.* **110** 053709
[10] Stringfellow G B 1986 *J. Cryst. Growth* **91** 75
[11] Kurtz S R, Olson J M, Kibbler A E and Asher S 1992 *InP & Related Mat. Conf.* vol 109 p 4

[12] Hudait M K, Modak P, Hardikar S and Krupanidhi S B 1997 *J. Appl. Phys.* **82** 4931
[13] Tokumitsu E 1990 *Japan. J. Appl. Phys.* **29** L698
[14] Walukiewicz W 1989 *Appl. Phys. Lett.* **54** 2094
[15] Seol J H, Moore A L, Saha S K, Zhou F, Shi L, Ye Q L, Scheffler R, Mingo N and Yamada T 2007 *J. Appl. Phys.* **101** 023706
[16] Karg S, Mensch P, Gotsmann B, Schmid H, Das Kanungo P, Ghoneim H, Schmidt V, Bjoerk M, Troncale V and Riel H 2012 *J. Electron. Mater.* at press
[17] Rode D L 1971 *Phys. Rev.* B **3** 3287
[18] Schenk A, Rhyner R, Luisier M and Bessire C D 2011 *Int'l Conf. Simulation of Semiconductor Processes and Devices (SISPAD)* vol 263
[19] Björk M T, Schmid H, Bessire C D, Moselund K E, Ghoneim H, Karg S, Lörtscher E and Riel H 2010 *Appl. Phys. Lett.* **97** 163501
[20] Karataev V V, Milvidskii M G, Rytova N S and Fistul V I 1977 *Sov. Phys.—Semicond.* **1** 1718
[21] Semikolenova N V, Nesmelova I M and Khabarov E N 1978 *Sov. Phys.—Semicond.* **12** 1139
[22] Noguchi M, Hirakawa K and Ikoma T 1991 *Phys. Rev. Lett.* **66** 2243
[23] Chen Y, Hermanson J C and Lapeyre G J 1989 *Phys. Rev.* B **39** 12682
[24] Thelander C, Dick K A, Borgström M T, Fröberg L E, Caroff P, Nilsson H A and Samuelson L 2010 *Nanotechnology* **21** 205703